Useful QCM Info

Kenneth R. Shull and Qifeng Wang

Contents

1 Introduction

This document accompanies the open source rheoQCM software written and maintained by Dr. Qifeng Wang at Northwestern University.

2 Background Theory

As the name implies, the quartz crystal microbalance (QCM) is most often employed as a high sensitivity mass-balance. The instrument relies on the piezoelectric nature of quartz to measure changes in resonance frequency caused by the application of a material to the quartz surface. An adsorbed mass or deposited film results in a decrease in resonant frequency of the quartz crystal by an amount, Δf_{sn}, that is given by the well-known Sauerbrey expression[1]:

$$\Delta f_{sn} = \frac{2n f_1^2}{Z_q} \Delta M_A = \frac{2n f_1^2}{Z_q} \rho_f d_f \tag{1}$$

Here, n is the order of the resonance harmonic, f_1 is the fundamental resonance frequency of quartz (5 MHz), Z_q is its acoustic shear impedance (8.84×10^6 kg/m^{2}s for AT cut quartz), ΔM_A is the mass per unit area of the film, ρ is its density and d is its thickness. Note that ρd is the mass per unit area.

Originally, the technique was designed for use in an air or vacuum environment, but today the QCM is often used to characterize molecules, particles and thin-films in liquid media. Applications include studies of adsorption[2–10], self-assembly[2–4], cell-substrate interactions[11], and electrochemistry[12, 13].

The QCM consists of a single-crystal quartz disc sandwiched between two electrodes. Due to the piezoelectric nature of quartz, the material will oscillate transversely if an alternating potential is applied across the electrodes, propagating a shear wave through the disc. If the frequency of oscillation is near to the acoustic resonance frequency of quartz, a standing shear wave will generate across the disc, inducing a peak in the system

conductance.[14, 15] For the AT-cut crystals used throughout this work, the fundamental resonant frequency is near 5 MHz. The conductance also peaks at odd harmonics (n) of the fundamental resonant frequency, with resonances at 15 MHz ($n=3$), 25 MHz ($n=5$), etc. If the conductance is plotted in the frequency domain, Lorentzian curves can be fit to the conductance peaks to provide two values: the resonance frequency (f_n), where the conductance is maximum at the nth harmonic, and the half-bandwidth (Γ_n), the half-width at half-maximum of the conductance peak. This half-bandwidth is equal to $2D/f_n$, where D is the dissipation factor introduced by the Chalmers group and utilized in the commonly employed time-domain QCM-D technique[16]. We refer to Γ_n simply as the dissipation, recognizing that our definition of the dissipation differs from the QCM-D definition by a factor of $2/f_n$.

If a load is applied to the QCM surface, f_n and Γ_n shift relative to the bare crystal and together make up a complex frequency shift[14, 15]:

$$\Delta f_n^* = \Delta f_n + i\Delta\Gamma_n \tag{2}$$

Note that in our notation, starred quantities are complex, and quantities subscripted with an n depend on the harmonic at which they are measured. When the frequency shift is small in comparison to the resonance frequency of quartz, which is true in nearly all applications of the QCM, Δf_n^* is related to the shift in complex load impedance (ΔZ_{nL}^*) through the small load approximation[14]:

$$\Delta f_n^* = \frac{if_1 \Delta Z_{nL}^*}{\pi Z_q} \tag{3}$$

2.1 Sauerbrey Limit

The Sauerbrey equation (Eq. 1) is obtained from Eq. 3, using the following inertial load impedance, ΔZ_{ns}^*, for ΔZ_{nL}^*:

$$\Delta Z_{sn}^* = 2\pi i n f_1 \rho_f d_f, \tag{4}$$

2.2 Bulk Limit

For thicker films, the complex resonant frequency deviates from the Sauerbrey relationship and depends on the rheological properties of the material in contact with the crystal surface. For films that are sufficiently thick (well beyond the decay length of the acoustic shear wave), the load impedance is equal to the acoustic impedance of a bulk material:

$$Z_{n,bulk}^* = (\rho G_n^*)^{1/2} \tag{5}$$

Here G_n^* is the complex shear modulus at f_n, expressed here in terms of its magnitude and phase angle:

$$G_n^* = |G_n^*|\exp(i\phi_n) \tag{6}$$

For a variety of reasons it is more convenient to express the complex shear modulus in terms of its magnitude and phase. The storage and loss moduli, G_n' and G_n'' respectively, can easily be obtained form the magnitude and phase:

$$\begin{aligned} G_n' &= |G_n^*|\cos(\phi_n) \\ G_n'' &= |G_n^*|\sin(\phi_n) \end{aligned} \tag{7}$$

Use of $Z_{n,bulk}^*$ for the load impedance gives the following for Δf_n and $\Delta\Gamma_n$ in the bulk limit:

$$\Delta f_n = -\frac{f_1}{\pi Z_q}\left(\rho |G_n^*|\right)^{1/2}\sin\left(\phi_n/2\right) \tag{8}$$

$$\Delta\Gamma_n = \frac{f_1}{\pi Z_q}\left(\rho |G_n^*|\right)^{1/2}\cos\left(\phi_n/2\right) \tag{9}$$

2

These equations can be inverted to give the following for $\rho \, |G_n^*|$ and ϕ

$$\rho \, |G_n^*| = \left(\frac{\pi Z_q \, |\Delta f_n^*|}{f_1} \right)^2 \tag{10}$$

$$\phi = 2 \arctan \left(\frac{\Delta f_n}{\Delta \Gamma_n} \right) \tag{11}$$

The decay length is given by the following expression:

$$\delta_n \rho = \frac{\rho}{\text{Im} \, (k^*)} = \frac{(\rho \, |G_n^*|)^{1/2}}{2 \pi n f_1 \sin (\phi_n / 2)} \tag{12}$$

We can use Eq. 8 to eliminate the sin term:

$$\delta_n \rho = \frac{(\rho \, |G_n^*|)}{2 \pi^2 n Z_q \Delta f_n} \tag{13}$$

Now we can use Eq. 10 to eliminate $\rho \, |G_n^*|$:

$$\delta_n \rho = -\frac{Z_q \, |\Delta f_n^*|^2}{2 n f_1^2 \Delta f_n} = -\frac{Z_q \, (\Delta f_n^2 + \Delta \Gamma_n^2)}{2 n f_1^2 \Delta f_n} \tag{14}$$

As a general rule of thumb, the bulk limit applies when the film thickness is larger than $\approx 2\delta_n$.

2.3   Generalized Single Layer

The complex wave vector, k_n^*, for shear wave propagation in the material can be obtained directly from Z_n^*[17]:

$$k_n^* = \frac{2 \pi f_n \rho}{Z_n^*} \tag{15}$$

The wavelength of the propagating shear wave is then obtained from the real part of k^* [17]:

$$\lambda_n = \frac{2\pi}{\text{Re} \, (k_n^*)}; \quad \lambda_n \rho = \frac{(\rho \, |G_n^*|)^{1/2}}{f_n \cos (\phi_n / 2)} \tag{16}$$

Finally, we define a quantity, D_n^*, which plays an important role in the expressions given below:

$$D_n^* = k_n^* d = \frac{2\pi d}{\lambda_n} \left(1 - i \tan (\phi_n / 2) \right) = \frac{2 \pi f_n d \rho}{Z_n^*} \tag{17}$$

The impedance of a layer (which we refer to hear as layer 1) of mass thickness $d\rho$ is given by the following expression:

$$Z_{n,film}^* = i Z_{n,bulk}^* \tan(D_n^*) \tag{18}$$

Note that we define Δf_{sn} as a positive number (see Eq. 1), so in the case where the Sauerbrey limit applies ($d / \lambda_n \ll 1$), and when there is sufficient acoustic contrast between the film and the surrounding liquid ($\left| Z_{nf}^* \right| \gg \left| Z_{n\ell}^* \right|$), we have $\Delta f_n^* = -\Delta f_{sn}$.

Figure 1: Two-layer geometry involving a 'film' that is sandwiched between the electrode surface and a 'membrane'.
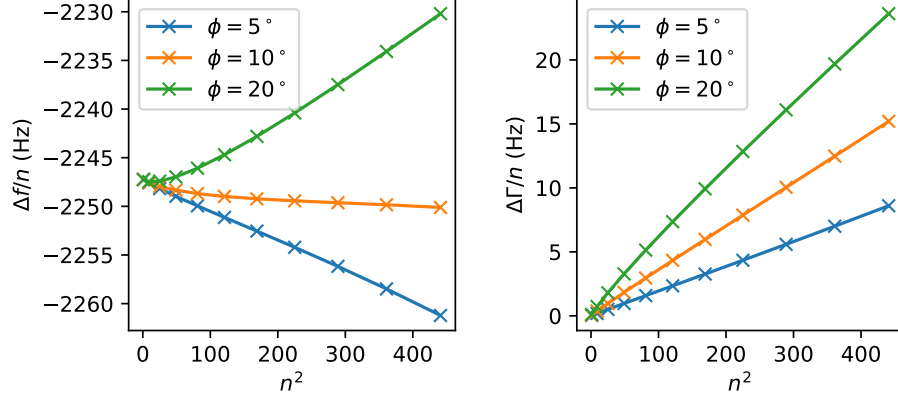

Figure 2: Result from the Lu-Lewis model for the parameters listed in Eqs. **??** and **??** varying the values of ϕ for the film as indicated.

2.4 Bilayer

We can apply Eq. 3, with $\Delta Z^*_{nL} = \Delta Z^*_{nfm}$ to get an expression for the complex frequency shift. After a bunch of algebra, we get to the following form of the master equation:

$$\frac{\Delta f^*_n}{f_{sn}} = -\frac{\tan(D^*_{n1})}{D^*_{n1}} \left[\frac{1 - \left(r^*_{n12}\right)^2}{1 + i r^*_{n12} \tan(D^*_{n1})} \right] \tag{19}$$

Where r^* is the ratio of the overall membrane impedance to the material impedance for the film:

$$r^*_{n12} = \frac{Z^*_{n2,film}}{Z^*_{n1,bulk}} \tag{20}$$

Written in this way it's a bit more obvious that there is no net response for the trivial case when a thin film and thick membrane have identical properties ($r^*_{n12} = 1$), and that the single layer master equation is recovered for experiments done in air ($r^*_{n12} = 0$).

In a liquid medium, the 'membrane' actually corresponds to a bulk, infinitely thick liquid. The impedance ratio is now a ratio of pure material properties:

$$r^*_{n12} = \left(\frac{\rho_2 G^*_{n2}}{\rho_1 G^*_{n1}} \right)^{1/2} \tag{21}$$

3 Lu-Lewis Equation

4 Thicker films

Things look quite a bit different if we use thicker films. Suppose we use a 5 μm glassy polymer film, representative of some of our experiments. Here's the set of film properties:
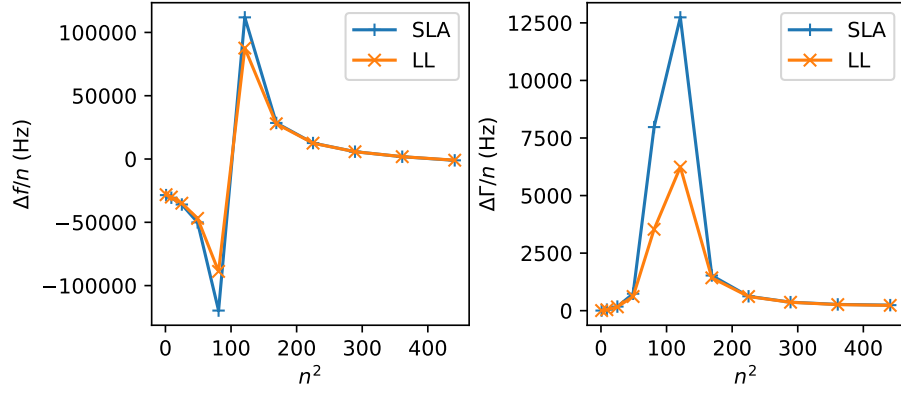
4

Figure 3: Comparison of the LL and SLA models for the electrode properties given in **??** and the film properties given in 22.
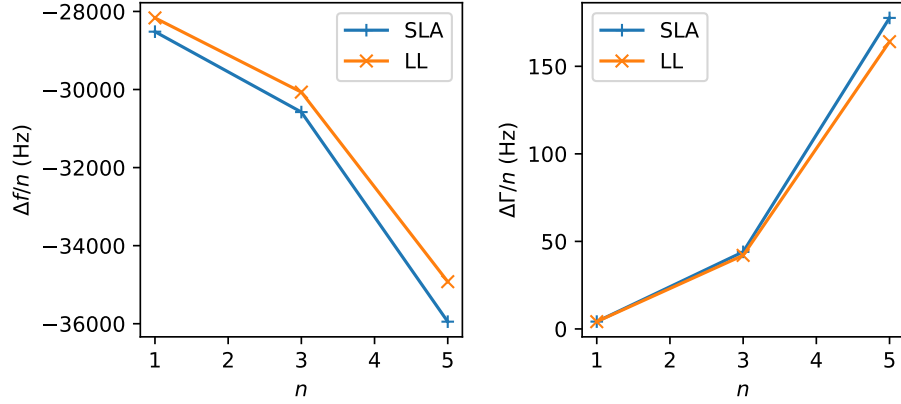

Figure 4: Comparison of the LL and SLA models for the electrode properties given in **??** and the film properties given in 22.

$$(d\rho)_{film} = 5\,\text{g/m}^2$$
$$(|G_3^*|\rho)_{film} = 10^9\,\text{Pa} \cdot \text{g/cm}^3 \tag{22}$$
$$\phi_{film} = 1.5°$$

Here's what the comparison of the LL and SLA models looks like in this case:

If we replot this as a function of linear n and just worry about the first few harmonics, it looks like the plot below.

5   Solution Method and Error Analysis

The numerical solution obtains three quantities (typically $d\rho$, $|G_3\rho|$ and ϕ) that give predicted three measured quantities in agreement with experimental values. These three measured quantities are two frequency shifts and one dissipation shift. In a $n_1 : n_2, n_3$ calculation, these quantities are Δf_{n1}, Δf_{n2} and $\Delta \Gamma_{n3}$. MATLAB and Python both return the Jacobian, J, at the solution point, which is given by the following expression:

$$J = \begin{bmatrix} \frac{\partial \Delta f_{n_1}}{\partial (d\rho)} & \frac{\partial \Delta f_{n_1}}{\partial (|G_3|\rho)} & \frac{\partial \Delta f_{n_1}}{\partial \phi} \\ \frac{\partial \Delta f_{n_2}}{\partial (d\rho)} & \frac{\partial \Delta f_{n_2}}{\partial (|G_3|\rho)} & \frac{\partial \Delta f_{n_2}}{\partial \phi} \\ \frac{\partial \Delta \Gamma_{n_3}}{\partial (d\rho)} & \frac{\partial \Delta \Gamma_{n_3}}{\partial (|G_3|\rho)} & \frac{\partial \Delta \Gamma_{n_3}}{\partial \phi} \end{bmatrix} \tag{23}$$

Once we have the matrix, we invert it to get J^{-1}, the Jacobian of the inverse function, which is what we need:

$$J^{inv} \equiv J^{-1} = \begin{bmatrix} \frac{\partial (d\rho)}{\partial \Delta f_{n_1}} & \frac{\partial (d\rho)}{\partial \Delta f_{n_2}} & \frac{\partial (d\rho)}{\partial \Delta \Gamma_{n_3}} \\ \frac{\partial (|G_3|\rho)}{\partial \Delta f_{n_1}} & \frac{\partial (|G_3|\rho)}{\partial \Delta f_{n_2}} & \frac{\partial (|G_3|\rho)}{\partial \Delta \Gamma_{n_3}} \\ \frac{\partial \phi}{\partial \Delta f_{n_1}} & \frac{\partial \phi}{\partial \Delta f_{n_2}} & \frac{\partial \phi}{\partial \Delta \Gamma_{n_3}} \end{bmatrix} \tag{24}$$

The uncertainties in the experimental quantities are Δf_{n1}^{err}, Δf_{n2}^{err} and $\Delta \Gamma_{n3}^{err}$. We represent these as three component error vector:

$$err = \left\{ \begin{array}{c} \Delta f_{n1}^{err} \\ \Delta f_{n2}^{err} \\ \Delta \Gamma_{n3}^{err} \end{array} \right\} \tag{25}$$

In our linearized analysis we just multiply the uncertainties by the appropriate partial derivatives, and sum the three different uncertainties in quadrature to get the associated experimental uncertainty in our extracted property:

$$\begin{aligned} (d\rho)^{err} &= \left(\left(J_{11}^{inv} err(1) \right)^2 + \left(J_{12}^{inv} err(2) \right)^2 + \left(J_{13}^{inv} err(3) \right)^2 \right)^{0.5} \\ (|G_3|\rho)^{err} &= \left(\left(J_{21}^{inv} err(1) \right)^2 + \left(J_{22}^{inv} err(2) \right)^2 + \left(J_{23}^{inv} err(3) \right)^2 \right)^{0.5} \\ \phi^{err} &= \left(\left(J_{31}^{inv} err(1) \right)^2 + \left(J_{32}^{inv} err(2) \right)^2 + \left(J_{33}^{inv} err(3) \right)^2 \right)^{0.5} \end{aligned} \tag{26}$$

This same analysis can be applied to more complicated models as well.

Bibliography

[1] G. Sauerbrey, Verwendung von Schwingquarzen zur Wägung dünner Schichten und zur Mikrowägung, Zeitschrift für Physik A Hadrons and Nuclei 155 (2) (1959) 206–222. doi:10.1007/BF01337937.

[2] K. A. Marx, Quartz Crystal Microbalance: A Useful Tool for Studying Thin Polymer Films and Complex Biomolecular Systems at the Solution-Surface Interface, Biomacromolecules 4 (5) (2003) 1099–1120. doi:10.1021/bm020116i.

[3] M. A. Cooper, V. T. Singleton, A survey of the 2001 to 2005 quartz crystal microbalance biosensor literature: applications of acoustic physics to the analysis of biomolecular interactions, Journal of Molecular Recognition 20 (3) (2007) 154–184. doi:10.1002/jmr.826.

[4] B. Becker, M. A. Cooper, A survey of the 2006-2009 quartz crystal microbalance biosensor literature, Journal of Molecular Recognition 24 (5) (2011) 754–787. doi:10.1002/jmr.1117.

[5] A. Tiraferri, P. Maroni, D. Caro Rodríguez, M. Borkovec, Mechanism of Chitosan Adsorption on Silica from Aqueous Solutions, Langmuir 30 (17) (2014) 4980–4988. doi:10.1021/la500680g.

[6] P. Yi, K. L. Chen, Release Kinetics of Multiwalled Carbon Nanotubes Deposited on Silica Surfaces: Quartz Crystal Microbalance with Dissipation (QCM-D) Measurements and Modeling, Environmental Science & Technology 48 (8) (2014) 4406–4413. doi:10.1021/es405471u.

[7] J. Song, W. E. Krause, O. J. Rojas, Adsorption of polyalkyl glycol ethers and triblock nonionic polymers on PET, Journal of Colloid and Interface Science 420 (2014) 174–181. doi:10.1016/j.jcis.2014.01.012.

[8] I. E. Salama, B. P. Binks, P. D. Fletcher, D. I. Horsup, Adsorption of benzyldimethyldodecylammonium chloride onto stainless steel using the quartz crystal microbalance and the depletion methods: an optimisation study, Colloids and Surfaces A: Physicochemical and Engineering Aspects 447 (2014) 155–165. doi:10.1016/j.colsurfa.2014.01.034.

[9] A. Rudrake, K. Karan, J. H. Horton, A combined QCM and XPS investigation of asphaltene adsorption on metal surfaces, Journal of colloid and interface science 332 (1) (2009) 22–31.

[10] Z. Liu, H. Choi, P. Gatenholm, A. R. Esker, Quartz Crystal Microbalance with Dissipation Monitoring and Surface Plasmon Resonance Studies of Carboxymethyl Cellulose Adsorption onto Regenerated Cellulose Surfaces, Langmuir 27 (14) (2011) 8718–8728. doi:10.1021/la200628a.

[11] J. Wegener, A. Janshoff, C. Steinem, The quartz crystal microbalance as a novel means to study cell-substrate interactions in situ, Cell Biochemistry and Biophysics 34 (1) (2001) 121–151.

[12] D. A. Buttry, M. D. Ward, Measurement of Interfacial Processes at Electrode Surfaces with the Electrochemical Quartz Crystal Microbalance, Chem. Rev. 92 (1992) 1355–1379.

[13] A. Hillman, The Electrochemical Quartz Crystal Microbalance, in: A. J. Bard, M. Stratmann, P. R. Unwin (Eds.), Encyclopedia of Electrochemistry, Volume 3, Instrumentation and Electroanalytical Chemistry, Vol. 3, Wiley-VCH, Weinheim, 2003, pp. 230–289.

[14] D. Johannsmann, Viscoelastic, mechanical, and dielectric measurements on complex samples with the quartz crystal microbalance, Physical Chemistry Chemical Physics 10 (31) (2008) 4516–4534.

[15] G. C. DeNolf, L. Haack, J. Holubka, A. Straccia, K. Blohowiak, C. Broadbent, K. R. Shull, High Frequency Rheometry of Viscoelastic Coatings with the Quartz Crystal Microbalance, Langmuir 27 (16) (2011) 9873–9879. doi:10.1021/la200646h.

[16] M. V. Voinova, M. Rodahl, M. Jonson, B. Kasemo, Viscoelastic Acoustic Response of Layered Polymer Films at Fluid-Solid Interfaces: Continuum Mechanics Approach, Physica Scripta 59 (5) (1999) 391–396. doi:10.1238/Physica.Regular.059a00391.

[17] F. Simonetti, P. Cawley, On the nature of shear horizontal wave propagation in elastic plates coated with viscoelastic materials, Proceedings of the Royal Society A: Mathematical, Physical and Engineering Sciences 460 (2048) (2004) 2197–2221. doi:10.1098/rspa.2004.1284.